Demonstration of the Highest Deuterium-Tritium Areal Density Using Multiple-Picket Cryogenic Designs on OMEGA

V. N. Goncharov,* T. C. Sangster, T. R. Boehly, S. X. Hu, I. V. Igumenshchev, F. J. Marshall, R. L. McCrory,† D. D. Meyerhofer,† P. B. Radha, W. Seka, S. Skupsky, and C. Stoeckl

Laboratory for Laser Energetics, University of Rochester, Rochester, New York 14623, USA

D. T Casey, J. A. Frenje, and R. D. Petrasso

Plasma Science and Fusion Center, Massachusetts Institute of Technology, Cambridge, Massachusetts 02139, USA

(Received 1 December 2009; published 20 April 2010)

The performance of triple-picket deuterium-tritium cryogenic target designs on the OMEGA Laser System [T. R. Boehly *et al.*, Opt. Commun. **133**, 495 (1997)] is reported. These designs facilitate control of shock heating in low-adiabat inertial confinement fusion targets. Areal densities up to 300 mg/cm^2 (the highest ever measured in cryogenic deuterium-tritium implosions) are inferred in the experiments with an implosion velocity $\sim 3 \times 10^7$ cm/s driven at peak laser intensities of 8×10^{14} W/cm^2. Extension of these designs to ignition on the National Ignition Facility [J. A. Paisner *et al.*, Laser Focus World **30**, 75 (1994)] is presented.

DOI: 10.1103/PhysRevLett.104.165001 PACS numbers: 52.57.−z

In inertial confinement fusion implosions a cryogenic shell of deuterium-tritium (DT) fuel is driven inward by means of direct or indirect laser illumination to achieve high compression and burn [1]. Fuel burn proceeds in two stages. First, a lower-density, higher-temperature (~10 keV) hot spot is formed by compression (PdV) work provided by higher-density, lower-temperature shell. Calculations show that to initiate burn, shell kinetic energy must exceed the threshold value [2], which depends on the shell implosion velocity $V_{\rm imp}$ (peak mass-averaged shell velocity), the in-flight shell adiabat $\alpha_{\rm if}$ (ratio of shell pressure to the Fermi-degenerate pressure at the peak shell density), and the drive pressure p_d. Second, as burn propagates through the fuel, shell inertia provides confinement time sufficient to burn a significant fraction of the assembled fuel. This requires fuel areal densities (ρR) at peak compression in excess of ~0.9 g/cm^2 [1]. The peak areal density in a direct-drive implosion depends on $\alpha_{\rm if}$ and laser energy E_L [3]:

$$\max(\rho R)_{\rm g/cm^2} = 2.6 \frac{E_{L,\rm MJ}^{1/3}}{\alpha_{\rm if}^{0.54}}. \quad (1)$$

Subscript MJ refers to megajoule energy units. To burn a sufficient fraction of fuel, the shell adiabat must be $\alpha_{\rm if} \leq 7E_{L,\rm MJ}^{0.6}$. While burn initiation physics requires laser energy in excess of ~300 kJ, which will be available on the National Ignition Facility (NIF) [4], implosions on the OMEGA laser [5] validate the ability of ignition designs to assemble cryogenic fuel with ignition-relevant implosion velocities ($V_{\rm imp} > 3 \times 10^7$ cm/s), maintaining the required fuel adiabat. A deviation of the adiabat from the designed value can be inferred by comparing the measured and predicted values of ρR. The areal density is determined by measuring spectral shapes of reaction products as they interact with the fuel [6,7]. This gives a value $\langle \rho R \rangle_n$ averaged over reaction time history. $\langle \rho R \rangle_n$ is calculated by using Eq. (1) with a numerical factor of 1.7 instead of 2.6 [3]. Then, an OMEGA cryogenic DT design, hydrodynamically equivalent to an $\alpha_{\rm if} = 2$ ignition design on the NIF, is predicted to achieve $\langle \rho R \rangle_n \sim 300$ mg/cm^2 at a laser energy of 30 kJ and a laser absorption fraction of ~70%, typical for OMEGA-scale targets. Reaching these areal densities on OMEGA, therefore, is a crucial step in validating predictive capabilities of hydrodynamic codes used to design ignition targets on the NIF.

The shell adiabat is determined by heating sources, including shock waves, radiation, and suprathermal electrons. Because of inaccuracies in the models used in target designing, experimental tuning is required to ensure that preheat is at an acceptable level. This Letter describes direct-drive target designs optimized for experimental shock timing to prevent adiabat degradation caused by excessive shock heating. This is accomplished by combining three intensity pickets with the main drive pulse [triple-picket (TP) design]. The main pulse in this case requires minimal shaping. Areal densities up to 300 mg/cm^2 are observed in cryogenic DT implosions on OMEGA using the TP designs driven at peak intensities $\sim 8 \times 10^{14}$ W/cm^2.

One of the main challenges in designing hot-spot ignition implosions is to control the generation of strong shocks while accelerating the fuel shell to $V_{\rm imp} > 3 \times 10^7$ cm/s. To avoid excessive shock heating, only few-Mbar shocks can be launched into cryogenic fuel at the beginning of an implosion. Preventing shell disruption due to the Rayleigh-Taylor instability [8], on the other hand, requires drive pressures p_d in excess of 100 Mbar since the

shell's in-flight aspect ratio $A_{\rm in}$ (ratio of shell radius R to shell thickness) is proportional to $p_d^{-2/5}$ [3] and shells with higher $A_{\rm in}$ are more susceptible to the perturbation growth during the acceleration phase. Pressure increase from a few Mbar to 100 Mbar can be achieved either adiabatically [continuous-pulse (CP) design] [9,10] or by launching a sequence of shocks of increasing strength [multiple-shock (MS) designs] [1,11].

Early cryogenic spherical implosions on OMEGA used the CP designs [12–15]. Both 5- and 10-μm-thick deuterated plastic (CD) shells with cryogenic 95-μm-thick D_2 and 80-μm-thick DT layers were used in these experiments. Areal densities close to the predicted values ($\langle\rho R\rangle_n \sim 130$ mg/cm^2) were achieved in implosions with 5 μm shells driven at peak intensities below $I_{\rm lim} = 3\times10^{14}$ W/cm^2 ($p_d \sim 50$ Mbar) and a laser pulse contrast ratio (CR) of less than 3.5. When 10 μm shells were used, $\langle\rho R\rangle_n \sim 200$ mg/cm^2 (80%–90% of the predicted values) were measured for designs with $I_{\rm lim} = 5\times10^{14}$ W/cm^2 ($p_d \sim 75$ Mbar) and CR < 30 [15]. The implosion velocity was $V_{\rm imp} \simeq 2.2\times10^7$ cm/s. Increasing drive intensities above $I_{\rm lim}$ resulted in significant deviations of measured and predicted $\langle\rho R\rangle_n$ [14]. Shock velocity measured in the CP designs using velocity interferometry system for any reflector (VISAR) [16] revealed difficulty in reproducing an adiabatic compression wave predicted in simulations [14,17]. Since the effect of steepening a compression wave into a shock, not predicted in simulations, is exacerbated by increasing either peak drive intensity or laser pulse CR, it is impractical to experimentally tune the adiabat in the CP designs to ignition-relevant values.

Initial fuel compression prior to reaching peak drive intensity can be accurately controlled in the MS designs by launching a sequence of shocks using intensity pickets. Next, we describe the main features of such designs. First, we assume that N shocks are launched by narrow intensity pickets, and the main shock is launched and supported by the main pulse. Since pressure of an unsupported shock decays in time, the fuel adiabat decreases from the front to the back of the shell. To account for spatial variation in the adiabat, $\alpha_{\rm if}$ must be replaced in Eq. (1) by adiabat at the inner shell surface $\alpha_{\rm inn}$ [3]. Indeed, the maximum shell convergence during an implosion is limited by a rarefaction wave, created at the main shock breakout time, with a tail propagating from the inner part of the shell toward the target center. This low-density tail is larger if $\alpha_{\rm inn}$ is higher. Later, as the main shock reflects from the center and begins interacting with the rarefaction, pressure at the target center starts to build up, initiating shell deceleration. Then, the larger $\alpha_{\rm inn}$ causes the main shell to decelerate farther from the center, reducing the final shell convergence and ρR.

Shocks from the pickets must compress the inner shell density to a value sufficient to keep the main shock from increasing $\alpha_{\rm inn}$ above the required value. Since inner density is reduced by a rarefaction wave launched at each shock breakout, density compression is maximized if all shocks break out of the shell nearly simultaneously (within $\Delta t \sim 5\%$ of the first shock propagation time). This relates the picket amplitudes and timing. For DT fuel, $\alpha \simeq p({\rm Mbar})/2.2\rho^{5/3}$, and the required inner shell compression after the main shock is $\rho_{\rm main}/\rho_0 \simeq 40[(p_d/100\ {\rm Mbar})/\alpha_{\rm inn}]^{3/5}$, where $\rho_0 = 0.25$ g/cm^3 is initial density. The density is compressed by a factor of 4 if the first shock pressure p_1 stays above $\sim$1 Mbar. Maximizing the density compression by remaining N shocks ($N-1$ shocks from pickets and the main shock) leads, with the help of Hugoniot relations [18], to a condition on shock pressure ratio as the shocks reach the inner surface, $p_{i+1} = p_i(p_d/p_1)^{1/N}$, where $i = 1,\ldots,N$. The inner adiabat in this case becomes

$$\alpha_{\rm inn} = 46\left(\frac{p_d}{100\ {\rm Mbar}}\right)\left[\frac{(p_d/p_1)^{1/N}+4}{4(p_d/p_1)^{1/N}+1}\right]^{5N/3}. \quad (2)$$

Radiation preheat and secondary compression waves, however, cause an additional increase (by a factor of 2–2.5) in $\alpha_{\rm inn}$. Then, the number of pickets N in a high-yield, direct-drive NIF design, is determined by setting $\alpha_{\rm inn} \simeq 1$ (this corresponds to an $\alpha \simeq 2.5$ CP design) in Eq. (2). This gives a relation between N and p_d, which is approximated by $p_d({\rm Mbar}) \simeq 6.5Ne^{0.78N}$. For $p_d \sim 100$ Mbar, $N = 3$, and pressures of the first three shocks, as they break out of the shell, are 1, 4.6, and 21 Mbar, respectively.

Next, a simple model is used to gain insight into the shock evolution in a multiple-picket design. A shock wave traveling along the x axis with a velocity $U_{\rm sh}$ is assumed to be sufficiently strong so that the flow velocity ahead of the shock can be neglected with respect to post-shock velocity in the laboratory frame of reference. Gradients in the flow created by unsupported shocks lead to PdV work on a fluid element, $d_t p \equiv \partial_t p + v\partial_x p = -(5/3)p\partial_x v$. The spatial gradient in velocity can be expressed in terms of pressure gradient and acceleration in the shock-front frame using Bernoulli's relation, $v\partial_x v + \partial_x p/\rho = -d_t U_{\rm sh} - \partial_t v$. In the strong-shock limit, $v = -U_{\rm sh}/4$ and $U_{\rm sh} = \sqrt{(4/3)p_s/\rho_0}$, leading to $d_t(p_s U_{\rm sh}^5) = -U_{\rm sh}^6(\partial_x p)_s$, where p_s is shock pressure and ρ_0 is density ahead of the shock. This equation can be simplified by introducing mass coordinate, $dm = \rho dx$, and replacing time with the mass m_s overtaken by the shock, $dm_s = \rho U_{\rm sh} dt$. At the shock front, this gives

$$\frac{d\ln(p_s U_{\rm sh}^5)}{dm_s} = -4\left(\frac{\partial \ln p}{\partial m}\right)_s. \quad (3)$$

According to a self-similar solution [19] and simulation results, the pressure behind the unsupported shock changes nearly linearly with mass, leading to solution of Eq. (3) in the form $p_s \sim m_s^{-1.14}\rho_0^{0.71}$. The first shock travels through uniform density, and its pressure decays as $p_1 \sim m_s^{-1.14}$. The post-shock adiabat varies as $\alpha_1 \sim m^{-1.14}$. Compared

to the results of self-similar solution [19], the error in the power index predicted by this model is within 10%. The density after the shock evolves as $\rho \sim (p/\alpha_1)^{3/5}$. Thus, the density ahead of the second-shock front grows as $\rho_0 \sim m_s^{1.29}$, and shock pressure decays as $p_2 \sim m_s^{-0.22}$. To generalize, if an $i+1$ shock with $p_{i+1} \sim m_s^{\delta_{i+1}}$ travels through the flow with an adiabat profile $\alpha_i \sim m^{-\omega_i}$, the model gives $\delta_{i+1} = 0.57\delta_i + 0.43$ and $\omega_{i+1} = 0.57\omega_i + 1.71$ with $\delta_1 = -\omega_1 = -1.14$. This shows that starting with the third shock, the pressure at the unsupported shock front increases as the shock travels through the shell. For the main shock (launched after N decaying shocks from the pickets) supported by pressure p_d, Eq. (3) gives (assuming again $p \sim m$) $p_{\text{main}} = p_d[3(\omega_N + 1)(m_s/m^*)^{\delta_{N+1}} - 8]/(3\omega_N - 5)$, where m^* is a normalization constant which depends on picket duration.

The model shows that the main shock pressure increases as the shock propagates through the shell, significantly exceeding the ablation pressure. To avoid an increase in α_{inn} due to this pressure amplification, it is necessary to either increase the number of pickets to 4 or reduce the strength of the main shock by introducing an intensity step at the beginning of the main drive. Because of short time separation between the last picket and the main drive in a quadruple-picket design, a combination of three pickets and a step pulse is chosen as a baseline for the multiple-picket, low-adiabat designs.

As described earlier, all shocks launched by the pickets and the main drive must coalesce nearly simultaneously. Leading shock velocity in this case decays prior to coalescence time at which the velocity experiences a sequence of 3 jumps up to $V_{\text{shock}} > 120$ μm/ns. Time separation between each jump in an OMEGA design is less than 50 ps. The measured velocity, therefore, is expected to increase continuously, as shown in Fig. 1 (dotted line). Because of the radiative precursor, the VISAR signal is absorbed in a region ahead of the shock front if $V_{\text{shock}} > 75$ μm/ns [20].

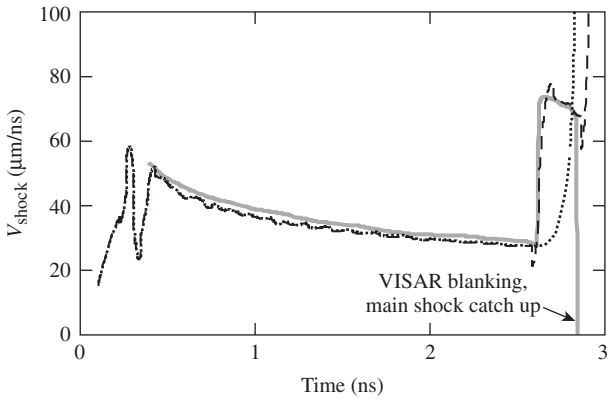

FIG. 1. Example of leading shock velocity history measured (thick solid line) and predicted (dashed line) in the TP design with a mistimed third shock. The calculated velocity history for an optimized design is shown by a dotted line.

Thus, only the first shock velocity and time of the coalescence sequence can be measured by the VISAR in an optimized design. Deviations from the optimal strength of any particular shock would result in early catch up of two shocks and lead to multiple velocity jumps, well separated in time and resolved by the VISAR measurement. For example, if the third picket is too high, the third shock will prematurely overtake the second and first shocks, resulting in a velocity jump up to 70 μm/ns. This is shown in Fig. 1 (dashed line) where two coalescence events are separated by 300 ps. Note that premature coalescence of the second and first shocks would lead to a smaller velocity jump (~ 50 μm/ns). Also shown in Fig. 1 is the result of VISAR measurement (solid line) which is in very good agreement with the predictions calculated using the one-dimensional hydrocode LILAC [21]. These experiments were performed on OMEGA with a 900-μm-diameter, 10-μm-thick CD shell filled with liquid D_2 and fitted with a VISAR cone [17].

To verify the shock optimization procedure and validate control of the main shock strength with an intensity step, the TP designs with both square- and a step-main pulses were used on the OMEGA Laser System to drive targets with a 65-μm-thick cryogenic DT layer overcoated with a 10-μm CD shell. The pulse shapes shown in Fig. 2 had a peak intensity of 8×10^{14} W/cm^2. The laser energy varied from 23 kJ for the square-main pulse to 25 kJ for the step-main pulse, respectively. The predicted implosion velocity in these designs reached 3×10^7 cm/s. A magnetic recoil spectrometer (MRS) [6] was used to infer $\langle \rho R \rangle_n$. Two charged-particle spectrometers were also used to measure the spectral shape of knock-on deuterons, elastically scattered by primary DT neutrons. The shape in the knock-on deuteron spectrum is insensitive, however, to areal densities above $\langle \rho R \rangle_n > 180$ mg/cm^2 [6]. These measurements were used to infer the lower limit on $\langle \rho R \rangle_n$ as well

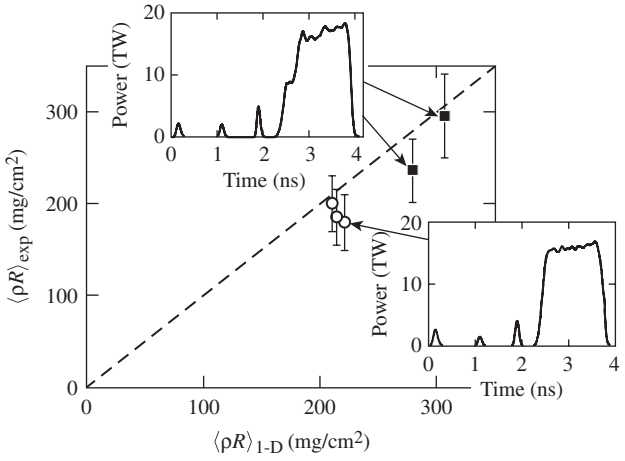

FIG. 2. Predicted and measured areal densities for triple-picket square (circles) and step (squares) OMEGA designs. The inserts show the pulse shapes used to drive the implosions.

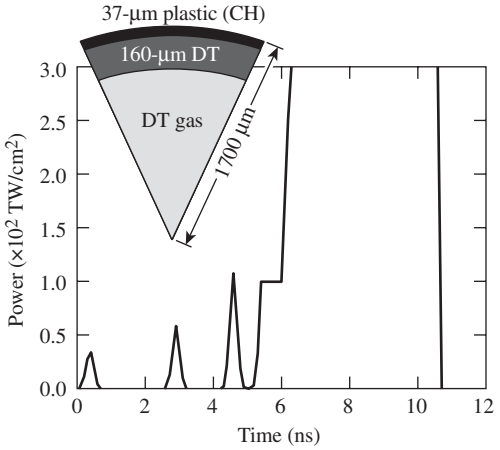

FIG. 3. Triple-picket, direct-drive design for the NIF.

as assess asymmetries developed at different views of an implosion. In Fig. 2 the measured areal densities are compared to those calculated using LILAC. Good agreement between measurements and calculations validates the accuracy of shock tuning in the TP designs. Also, the observed increase in $\langle \rho R \rangle_n$ in the step design confirms that the inner adiabat can be accurately controlled by changing step amplitude in the main drive.

Based on the good performance of the TP designs on OMEGA, a new direct-drive-ignition design is proposed for the NIF (Fig. 3). Driven at a peak intensity of 8×10^{14} W/cm^2, the shell reaches $V_{\mathrm{imp}} = (3.5\text{–}4) \times 10^7$ cm/s, depending on the thickness of the fuel layer. At a laser energy of 1.5 MJ this design is predicted to ignite with a gain $G = 48$. The stability assessment of the NIF TP design is currently in progress.

In summary, triple-picket designs were used in cryogenic DT implosions on OMEGA. The highest areal densities ever measured in cryogenic DT implosions (up to 300 mg/cm^2) were inferred with $V_{\mathrm{imp}} \sim 3 \times 10^7$ cm/s driven at a peak laser intensity of 8×10^{14} W/cm^2. Scaled to the NIF, the TP design is predicted to ignite with a gain $G = 48$.

This work was supported by the U.S. Department of Energy Office (DOE) of Inertial Confinement Fusion under Cooperative Agreement No. DE-FC52-08NA28302, the University of Rochester, and the New York State Energy Research and Development Authority. The support of DOE does not constitute an endorsement by DOE of the views expressed in this Letter.

*Also with: Department of Mechanical Engineering, University of Rochester, Rochester, NY 14623, USA.
†Also with: Department of Mechanical Engineering and Department of Physics and Astronomy, University of Rochester, Rochester, NY 14623, USA.

[1] J. D. Lindl, *Inertial Confinement Fusion* (Springer, New York, 1998).
[2] M. C. Herrmann, M. Tabak, and J. D. Lindl, Phys. Plasmas **8**, 2296 (2001).
[3] C. D. Zhou and R. Betti, Phys. Plasmas **14**, 072703 (2007).
[4] J. A. Paisner, J. D. Boyes, S. A. Kumpan, W. H. Lowdermilk, and M. S. Sorem, Laser Focus World **30**, 75 (1994).
[5] T. R. Boehly *et al.*, Opt. Commun. **133**, 495 (1997).
[6] J. A. Frenje *et al.*, Phys. Plasmas **16**, 042704 (2009).
[7] F. Seguin *et al.*, Phys. Plasmas **9**, 2725 (2002).
[8] S. Chandrasekhar, *Hydrodynamic and Hydromagnetic Stability* (Claredon, Oxford, 1961), p. 428.
[9] P. W. McKenty, V. N. Goncharov, R. P. J. Town, S. Skupsky, R. Betti, and R. L. McCrory, Phys. Plasmas **8**, 2315 (2001).
[10] V. N. Goncharov *et al.*, Phys. Plasmas **10**, 1906 (2003).
[11] J. D. Lindl and W. C. Mead, Phys. Rev. Lett. **34**, 1273 (1975).
[12] F. J. Marshall *et al.*, Phys. Plasmas **12**, 056302 (2005).
[13] T. C. Sangster *et al.*, Phys. Plasmas **14**, 058101 (2007).
[14] V. A. Smalyuk *et al.*, Phys. Plasmas **16**, 056301 (2009).
[15] T. C. Sangster *et al.*, Phys. Rev. Lett. **100**, 185006 (2008).
[16] L. M. Barker and R. E. Hollenbach, J. Appl. Phys. **43**, 4669 (1972).
[17] T. R. Boehly *et al.*, Phys. Plasmas **16**, 056302 (2009).
[18] L. D. Landau and L. M. Lifshitz, *Fluid Mechanics* (Pergamon, New York, 1982).
[19] Ya. B. Zeldovich and Yu. P. Raiser, *Physics of Shock Waves and High-Temperature Hydrodynamic Phenomena* (Dover, New York, 2002), p. 820.
[20] D. H. Munro *et al.*, Phys. Plasmas **8**, 2245 (2001).
[21] J. Delettrez, R. Epstein, M. C. Richardson, P. A. Jaanimagi, and B. L. Henke, Phys. Rev. A **36**, 3926 (1987).